Steel and Composite Structures, *Vol. 20, No. 1 (2016) 91-106*
DOI: http://dx.doi.org/10.12989/scs.2016.20.1.091

Load-carrying capacity degradation of reinforced concrete piers due to corrosion of wrapped steel plates

Shengbin Gao [1], Toyoki Ikai [2], Jie Ni [3] and Hanbin Ge [*2]

[1] *Department of Civil Engineering, School of Naval Architecture, Ocean and Civil Engineering, Shanghai Jiao Tong University, Shanghai, 200240, China*
[2] *Department of Civil Engineering, Meijo University, Nagoya, 468-8502, Japan*
[3] *The IT Electronic 11th Design & Research Institute, Shanghai, 200233, China*

(*Received June 18, 2015, Revised September 25, 2015, Accepted September 26, 2015*)

Abstract. Two-dimensional elastoplastic finite element formulation is employed to investigate the load- carrying capacity degradation of reinforced concrete piers wrapped with steel plates due to occurrence of corrosion at the pier base. By comparing with experimental results, the employed finite element analysis method is verified to be accurate. After that, a series of parametric studies are conducted to investigate the effect of corrosion ratio and corrosion mode of steel plates located near the base of in-service pier P2 on load-carrying capacity of the piers. It is observed that the load-carrying capacity of the piers decreases with the increase in corrosion ratio of steel plates. There exists an obvious linear relationship between the load-carrying capacity and the corrosion ratio in the case of even corrosion mode. The degradation of load-carrying capacity resulted from the web's uneven corrosion mode is more serious than that under even corrosion mode, and the former case is more liable to occur than the latter case in actual engineering application. Finally, the failure modes of the piers under different corrosion state are discussed. It is found that the principal tensile strain of concrete and yield range of steel plates are distributed within a wide range in the case of slight corrosion, and they are concentrated on the column base when complete corrosion occurs. The findings obtained from the present study can provide a useful reference for the maintenance and strengthening of the in-service piers.

Keywords: bridge engineering; reinforced concrete pier; wrapped steel plate; corrosion ratio; corrosion mode; load-carrying capacity degradation

1. Introduction

Steel-concrete composite structures have been extensively used in civil and building fields due to the best combination of strong tensile strength for steel with excellent compression strength for concrete. However, the main disadvantages of steel can attribute to its weak ability to resist fire and corrosion. With respect to steel reinforced concrete (SRC) columns and concrete-filled steel columns, extensive researches on fire and seismic performance have been carried out in the past few years. Han *et al*. (2015) developed a three-dimensional finite element analysis modeling to investigate the performance of SRC columns under fire. Extensive parametric studies were performed to identify the key parameters influencing the fire resistance of the SRC column. As a

*Corresponding author, Professor, E-mail: gehanbin@meijo-u.ac.jp

http://www.techno-press.org/?journal=scs&subpage=8 ISSN: 1229-9367 (Print), 1598-6233 (Online)

consequence, a simplified calculation method was proposed to predict the fire resistance of the SRC column. Kang *et al*. (2015) recalibrated the capacity reduction factors, estimated the reliability of current equations, and investigated the effect of these factors in AS 5100.6, the Australian Bridge Standard for concrete-filled steel tubular columns. It was concluded that the current capacity factor values in AS 5100 were adequate with regards to safety, but better optimized values would be preferable to improve the cost-safety balance. Fan *et al*. (2014) tested six three-dimensional (3D) joints between concrete-filled square steel tubular columns and composite steel-concrete beams under bidirectional reversal loads to investigate the seismic performance of these composite joints. The test specimens exhibited good strength and stiffness retention capacities and excellent energy dissipation. The typical failure mode of the specimens was shear damage of the joint panel. The influence of the bidirectional loading was minor during the initial response of the joint in elastic range, but it became significant when the joint was loaded into plastic range.

Reinforced concrete piers wrapped with steel plates have been widely used in highway with the advantages of high load-carrying capacity and strong energy-dissipation capacity (Wan and Han 1995). However, it is found that the steel plates near the pier base and the holes for infilling the bonding paste are liable to corrode due to waterlogging and other corrosion environment in practical applications (see Fig. 1). Up to date, a lot of researches on general mechanical behavior degradation of the structures due to steel corrosion have been investigated. Fang and Kou (2005) studied the effect of rebar corrosion on bond strength in concrete structures by carrying out some axial loading tests on corroded stub columns. Sharifi and Paik (2011) developed a procedure to assess the ultimate strength reliability of box girder bridge with the degradation of plate members due to general corrosion. A probabilistic model to predict ultimate strength of steel box girder was established based on an analytical formula that accounts for corrosion-related, time-dependent strength degradation. Silva and Garbatov (2013) investigated the effects of a random corrosion thickness distribution on the ultimate strength of unstiffened rectangular steel plates subjected to uniaxial compressive load. Based on a regression analysis, empirical formulae to predict strength reduction due to corrosion was derived. Hou *et al*. (2013) carried out a full-range analysis on the CFST stub columns and beams subjected to both loading and chloride corrosion. Simplified methods to calculate the strength of CFST stub column and beam under long-term loading and corrosion were illustrated on the basis of parameter analysis. Khedmati *et al*. (2011) introduced the effects of general corrosion on both sides of the steel plates into the finite element models using a random thickness surface model, and evaluated the corrosion effects on plate compressive strength as a result of parametric variation of the corroded surface geometry. A proposal on the effective thickness was offered to estimate the ultimate strength and explore the post-buckling behavior of randomly corroded steel plates under uniaxial compression. Kaita *et al*. (2012) proposed a simple and accurate method to calculate the remaining yield and tensile strength by using a concept of representative effective thickness with correlation of initial thickness and maximum corroded depth, based on the results of many tensile coupon tests of corroded plates obtained from a steel plate girder with severe corrosion. A strength reduction diagram was presented for bridge inspection engineers to make rational decisions about the maintenance management of aged steel bridge infrastructures.

The corrosion pattern considered in the above-mentioned researches is general corrosion, which cannot consider the effect of corrosion position, or corrosion range and so on. However, the phenomenon that corrosion occurs on the total surface of steel members at the same time is rather few in practical applications, the more is localized corrosion instead. Wang and Liu (2012) carried

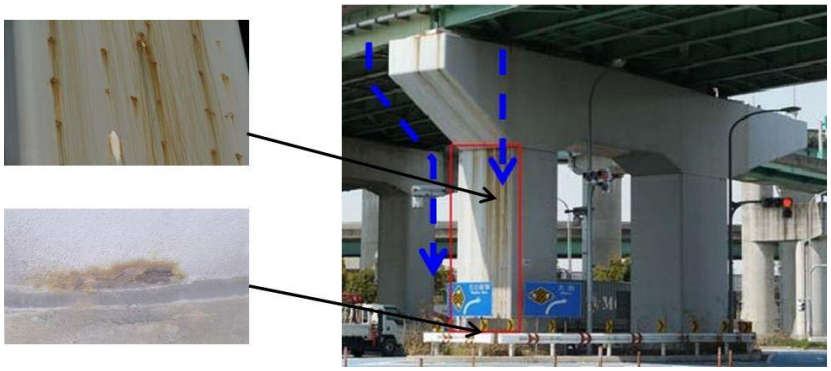

Fig. 1 Corrosion phenomenon observed in reinforced concrete pier wrapped with steel plates

out tests to investigate the effects of length and location of rebar corrosion on structural behavior and load-carrying capacity of reinforced concrete columns. It was concluded that the load-carrying capacity of corroded RC columns were affected by the location of the partial length, the corrosion level within partial length and the asymmetrical deterioration of the concrete section. Karagah *et al*. (2015) tested a total of 13 H-shaped short columns under monotonic axial load to investigate the effect of corrosion on the axial capacity of steel bridge piles. To simulate the corrosion, webs and flanges were milled near the mid-height of the columns to adjust their plate thicknesses. The test results were compared with the axial capacities predicted by some design provisions. It was found that flange corrosion had the most significant effect on the column capacity. Shi *et al*. (2014) carried out numerical simulation to evaluate the capacity of steel bridge piles with localized severe corrosion. A parametric study was conducted to analyze different factors that affected the axial capacity and failure mode of these piles. A damage classification system was proposed based on the remaining capacity of the corroded pile. Zhang (2011) carried out numerical analysis to investigate the effect of different corrosion patterns on ultimate strength and deformation capacity of axial compressed CFT stub columns. It was found that local corrosion had a more serious effect than general corrosion.

Up to now, the researches on corroded steel bridge piers are scarce. This paper is aimed to investigate the load-carrying capacity degradation of reinforced concrete piers due to corrosion of wrapped steel plates near the pier base. Firstly, the accuracy of the employed two-dimensional elastoplastic finite element analysis method is verified by comparing with experimental results. Then, a series of parametric studies are carried out to clarify the effect of corrosion ratio and corrosion mode of steel plates on load-carrying capacity of the in-service pier. Finally, the failure modes at different corrosion level are discussed from the viewpoint of the principal tensile strain of concrete and yield range of steel plates. The research results are expected to provide a useful reference for the maintenance and strengthening of the in-service piers.

2. Test verification of the analytical method

2.1 Introduction to test specimens

As shown in Fig. 2, three reinforced concrete bridge piers with square section (600 mm × 600 mm) are analyzed (Saito *et al*. 1996). Fig. 2(a) shows an original reinforced concrete pier (Case A).

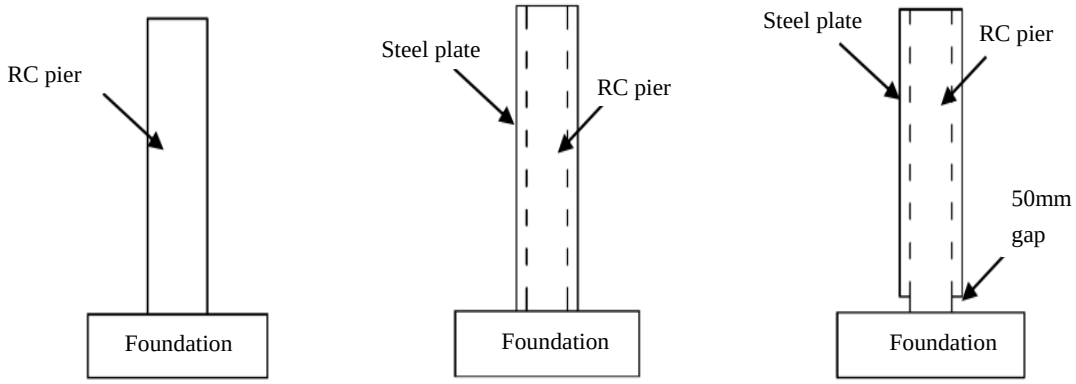

(a) Case A (b) Case B (c) Case C

Fig. 2 Sketch of test specimens

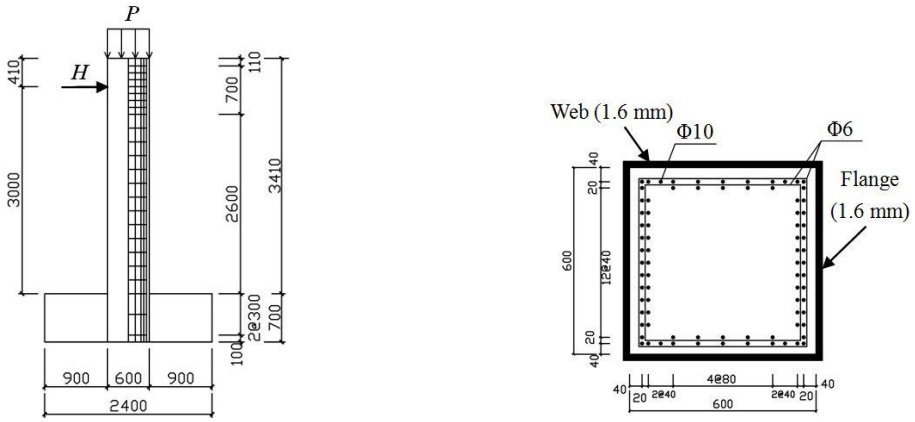

(a) Elevation plan (b) Cross section

Fig. 3 Geometry dimensions of test specimens

The pier illustrated in Fig. 2(b) is wrapped with steel plates (Case B), in which the steel plates are fully connected with the foundation. Fig. 2(c) also shows a reinforced concrete pier wrapped with steel plates (Case C). But the difference between Case B and Case C lies in that there exists a 50 mm-height gap between steel plates and foundation in the latter case. Case C is taken to simulate the complete corrosion state of steel plates near the pier base, while Case B is looked as an uncorroded pier. The elevation plan and cross section of the test specimens are given in Fig. 3. The height of the specimen is 3410 mm, and the steel plates used for both flange and web is 1.6 mm in thickness. Rebar assignment of the specimens is given in Fig. 3(b) with 1.6% of longitudinal rebar ratio.

2.2 Finite element model

The thickness of steel plates used for strengthening the reinforced concrete piers is very thin compared with that employed in the concrete-filled steel columns. Therefore, the confined effect of wrapped steel plates on the improvement of concrete compressive strength cannot be expected

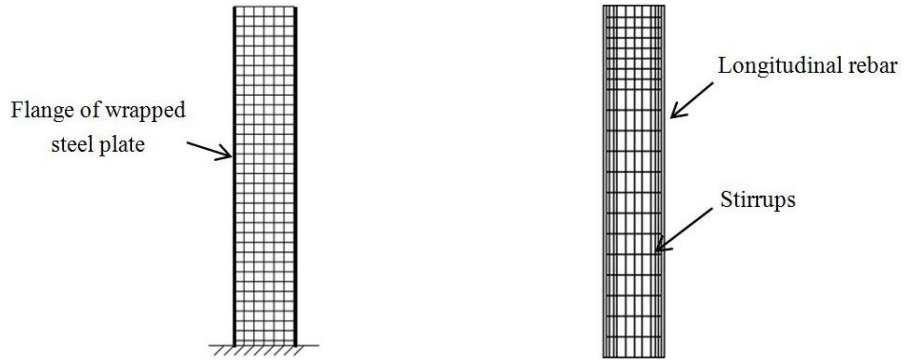

(a) Steel plate and concrete (b) Rebar

Fig. 4 Finite element mesh of test specimens

so much. To simplify the finite element analysis modelling, 2-D analytical models of the test specimens are established by using ABAQUS software package (2010), as shown in Fig. 4. Four-node plane stress element is employed to model concrete and steel web, respectively. Beam-column element is used to model steel flange. Truss element is used to model longitudinal rebars and stirrups, which are fully embedded in concrete elements. All the steel plates are assumed to work together with the adjacent concrete elements.

2.3 Material properties

Table 1 gives material properties of rebar, stirrup, steel plate and concrete. A perfectly elaso-plastic model is employed for rebar and stirrup. A strain hardening model with yield plateau is used to model uniaxial stress-strain relationship of steel plates (Gao and Ge 2007). As for concrete, a damage-based elastoplastic model is used. Fig. 5 shows a uniaxial stress-strain relationship of concrete subjected to compression, which was proposed by Maekawa *et al*. (1993) as follows

$$\sigma = E_0 K\left(\varepsilon - \varepsilon_p\right) \tag{1}$$

$$E_0 = \frac{2f_c}{\varepsilon_{peak}} \tag{2}$$

$$K = \exp\left\{-0.73\frac{\varepsilon}{\varepsilon_{peak}}\left(1 - \exp\left(-1.25\frac{\varepsilon}{\varepsilon_{peak}}\right)\right)\right\} \tag{3}$$

$$\varepsilon_p = \varepsilon - 2.86\varepsilon_{peak}\left(1 - \exp\left(-0.35\frac{\varepsilon}{\varepsilon_{peak}}\right)\right) \tag{4}$$

in which, ε is current strain, K is the remaining ratio of elastic stiffness, $\varepsilon_{\text{peak}}$ is the strain corresponding to compressive strength (taken as 0.002 in general), ε_p is plastic strain. A linear tensile softening model is adopted to simulate the concrete cracking, and the ultimate strain corresponding to zero tensile stress is equal to the yield strain of rebar.

Table 1 Material properties (unit: MPa)

	Rebar		Stirrup		Steel plate		Concrete	
	Test	Pier P2	Test	Pier P2	Test	Pier P2	Test	Pier P2
Young's modulus	2.06×10^5	2.06×10^5	2.06×10^5	2.06×10^5	2.06×10^5	2.06×10^5	2.78×10^4	2.78×10^4
Yield stress	381	180	328	180	235	235	—	—
Tensile stress	—	—	—	—	—	—	3.0	3.0
Compressive strength	—	—	—	—	—	—	38.3	30.8

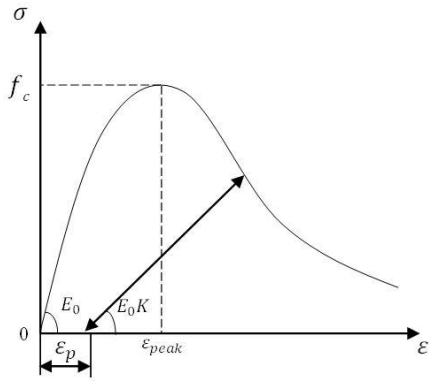

Fig. 5 Uniaxial stress-strain relation of concrete

2.4 Loads and boundary condition

A constant vertical load (P = 550 kN) is applied first at the pier top, followed by an incremental lateral displacement applied at the position with 410 mm far away from the pier top, as shown in Fig. 3(a). The pier base is fully fixed, that is to say, all degrees of freedom of both concrete and steel plates at the pier base are constrained.

2.5 Comparisons of analytical results with test results

Figs. 6(a)-(c) compares the lateral load versus lateral displacement curves obtained from numerical analysis with the test results. It is observed that both the peak load and post-peak curves obtained from present analysis coincide well with the test results although there exist some differences in the initial stiffness. This difference attributes to the assumption that the pier base is fully fixed with the foundation in the analysis, which cannot be completely fulfilled in the test. With respect to the corrosion state, Case B represents the uncorroded pier, the maximum strength of which is almost 100 kN larger than that of Case A. This indicates that the strengthening method to wrap steel plates outside the reinforced concrete pier can significantly improve the load-carrying capacity of the piers. In contrast, Case C refers to the corroded pier, of which the steel plates near the pier base fully corrode. By comparing the lateral load - lateral displacement curves of Case C with that of Case A, almost the same maximum strengths are observed, which means that the wrapped steel plates cannot make any obvious contribution to the load-carrying capacity if the steel plates near the pier base completely corrode.

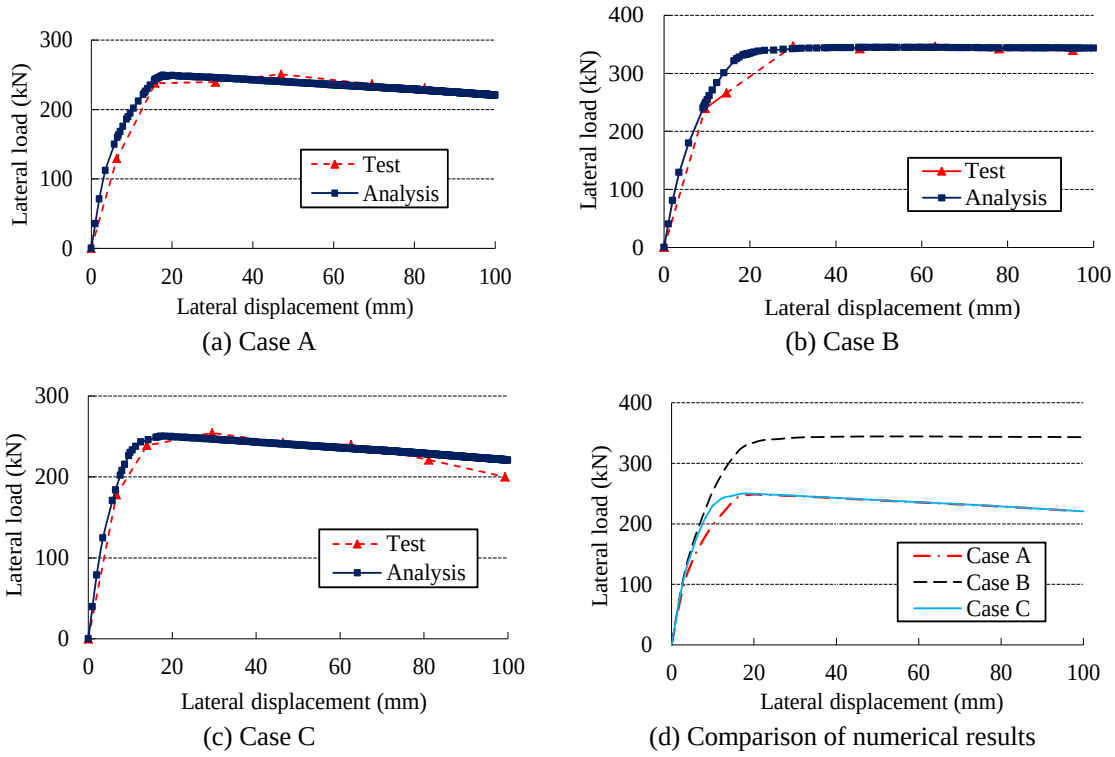

Fig. 6 Comparison of lateral load - lateral displacement curves

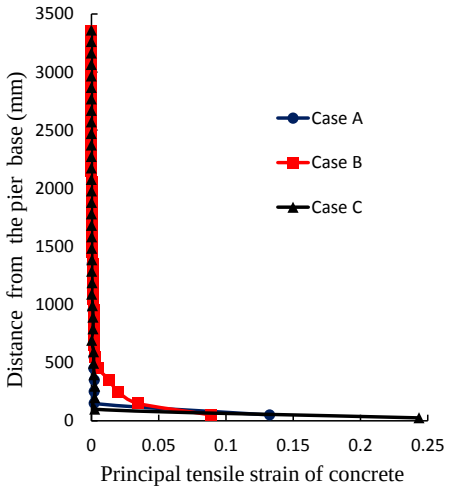

Fig. 7 Comparison of principal tensile strain distribution of concrete

Fig. 7 shows the distribution diagrams for principal tensile strain of concrete along tensile side from bottom to top of three tested specimens. It is observed that the maxium tensile strain of Case A, Case B, and Case C reaches 0.132, 0.089, and 0.243, respectively. Compared with Case A and

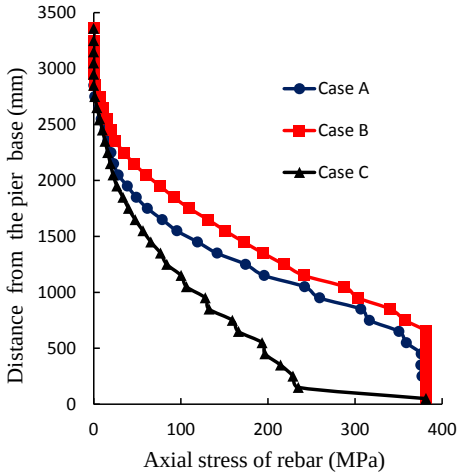

Fig. 8 Comparison of axial stress distribution of tensile rebar

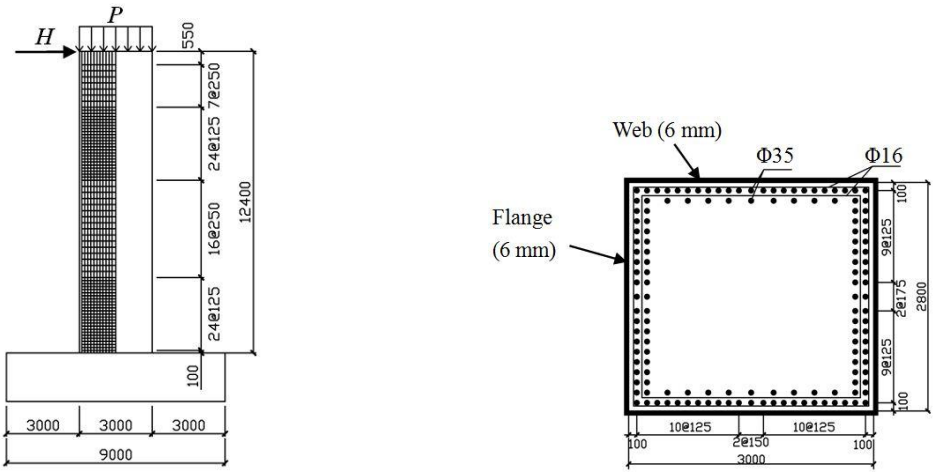

(a) Elevation plan (b) Cross section

Fig. 9 Geometry dimensions of in-service pier P2

Case C, the principal tensile strain of concrete in Case B distributes in a relatively wide range from the pier base.

Fig. 8 compares the axial stress distribution of rebar along tensile side from bottom to top of three tested specimens. It is found that the rebars yield within a large range in Case A and Case B, while the yield range in Case C is very limited. The above-mentioned comparisons of principal tensile strain distribution of concrete and axial stress distribution of tensile rebar demonstrate that the completely corroded steel plates in Case C result in local deformation at the pier base and significantly reduce the load-carrying capacity of the piers.

3. Corrosion analysis of in-service pier

3.1 Introduction to in-service pier

Fig. 9 shows the elevation plan of an in-service pier (hereinafter referred to as P2). 42 longitudinal rebars (Φ35) are arranged adjacent to each flange corresponding to 1.5% of longitudinal rebar ratio, and the stirrups adopted are Φ16. The cross section of pier P2 is 2800 mm (flange) × 3000 mm (web), and the total height of which is 12400 mm. The steel plate used for wrapping is 6 mm in thickness. After applying a constant vertical load of 11090 kN at the pier top, an incremental displacement is followed till the failure of the pier.

2-D elastoplastic finite element model is established. The selection of element type and the analytical method are the same as those described in Sections 2.2-2.4, which are omitted here. The material properties of steel plate, rebar, and concrete are given in Table 1.

The analytical cases given in Table 2 consist of the following three types. The first type is the original reinforced concrete pier (P2). The second type is the pier wrapped with steel plates without any corrosion (P2-F00W00). The third type is to consider the effect of steel plates' corrosion at the pier base by introducing a parameter of corrosion ratio. The corrosion ratio k_t in the case of even corrosion mode is defined as follows

$$k_t = \frac{t_0 - t_1}{t_0} \times 100\% \tag{5}$$

in which, t_0 is the thickness of steel plate without corrosion, and t_1 is the remaining thickness of corroded steel plate. The web corrosion ratio k_w in the case of uneven corrosion mode is defined as follows

$$k_w = \frac{d_0 - d_1}{d_0} \times 100\% \tag{6}$$

in which, d_0 is the web width, and d_1 is the remaining web width after corrosion.

It should be noted that the same corrosion modes as those adopted in this paper do not exist in actual steel piers. In fact, corrosion distribution is very irregular no matter along plate surface or along plate thickness. This complexity of corrosion is very difficult to be accounted for in finite

Table 2 Analytical cases of P2 under even corrosion mode

Specimen	Corrosion ratio along flange's thickness k_t (%)	Corrosion ratio along web's thickness k_t (%)	Specimen	Corrosion ratio along flange's thickness k_t (%)	Corrosion ratio along web's thickness k_t (%)
P2-F00W00	0	0	P2-F100W20	100	20
P2-F20W00	20	0	P2-F100W40	100	40
P2-F40W00	40	0	P2-F100W60	100	60
P2-F60W00	60	0	P2-F100W80	100	80
P2-F80W00	80	0	P2-F100W100	100	100
P2-F100W00	100	0	P2	—	—

element modeling unless some assumptions must be made to simplify or idealize the corrosion distribution, especially in 2-D finite element modeling which is employed in this paper. However, such assumption on corrosion mode is considered to be safe because the critical cases have been covered.

3.2 Even corrosion analysis of in-service pier

In this section, a series of parametric studies are carried out to investigate the effect of steel plate's corrosion ratio on the load-carrying capacity of the piers. The corroded range of steel plates is limited within 100 mm height from the pier base. The analytical cases are listed in Table 2. Here, taking "P2-F100W20" as an example to illustrate the naming rules of each specimen, "F" represents the tensile flange, and "W" denotes web. "100" followed by"F"means complete corrosion along flange thickness, and "20" followed by"W"indicates that 20% of web thickness corrodes. Except for P2, all other specimens are wrapped with steel plates.

In order to accurately evaluate the strength degradation of the specimens, both the maximum strength (H_m) and the ultimate strength (H_u) are employed. As shown in Fig. 10, the maximum strength refers to the peak load, while the ultimate strength corresponds to the lateral displacement with 1/50 of the specimen height on the basis of Building Seismic Design Specification (GB-2010) in China. The degradation of ultimate strength can well reflect the post-peak behavior after corrosion of steel plates.

Fig. 11(a) shows comparison of lateral load - lateral displacement curves of the specimens with different corrosion ratio of flange. It is observed that with the increase of corrosion ratio, the maximum strength of the specimens gradually decreases. Fig. 11(b) gives comparison of lateral load - lateral displacement curves of the specimens with different corrosion ratio of web and complete corrosion on flange. For comparison, the corresponding numerical result of original pier P2 is also given. We can see that with the increase in corrosion ratio of web, the maximum strength of the specimens decrease rapidly. When the corrosion ratio reaches 100% (see P2-F100W100), the maximum strength of the specimen becomes almost the same as that of the original pier P2. From this point of view, corrosion of steel plates displays significant influence on the maximum strength of the piers.

Fig. 12 shows the relationship between corrosion ratio and the load-carrying capacity of the piers. Both the maximum strength and ultimate strength decrease linearly as the increase of

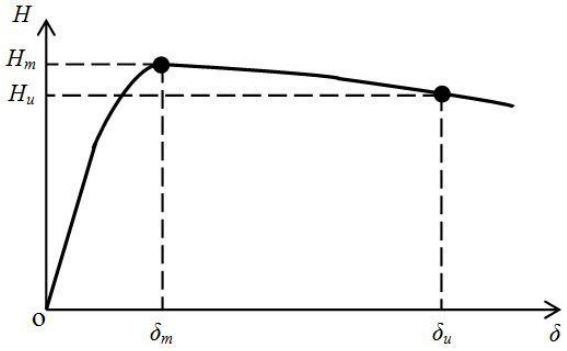

Fig. 10 Definition of maximum strength and ultimate strength

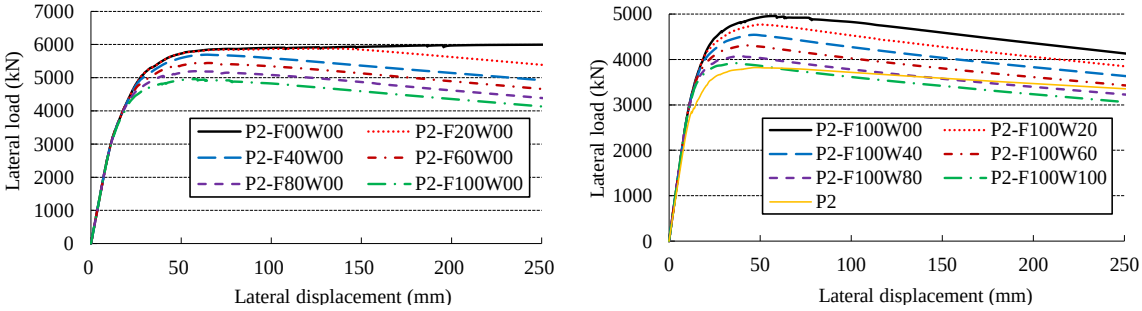

(a) Different corrosion ratio of flange (b) Different corrosion ratio of web

Fig. 11 Comparison of lateral load - lateral displacement curves corresponding to different corrosion ratio

corrosion ratio. Table 3 lists the analytical results of maximum strength and ultimate strength, as well as the improvement percentage of maximum strength, degradation ratio of maximum strength and ultimate strength due to corrosion. By comparing the results of specimens P2-F00W00 (No corrosion on steel plates), P2-F100W00 (Complete corrosion on flange only), P2-F100W100 (Complete corrosion on steel plates), and P2 (Original pier), the maximum strength of specimen P2-F00W00 is improved by 56.9% compared with that of specimen P2. When the steel plates near the pier base completely corrode (see P2-F100W100), the maximum strength is only increased by 2.7%. Therefore, to what extent the maximum strength of the specimens deteriorates mainly depends on the corrosion state of the steel plates. Degradation ratio of load-carrying capacity increases rapidly as the corrosion on flange and web becomes serious. As shown in Table 3, degradation ratio of the ultimate strength is always larger than that of the maximum strength,

Table 3 Analytical results under even corrosion mode

Specimens	Maximum strength (kN)	Ultimate strength (kN)	Improvement percentage of maximum strength (Compared with P2)	Degradation ratio of maximum strength due to corrosion (Compared with P2-F00W00)	Degradation ratio of ultimate strength due to corrosion (Compared with P2-F00W00)
P2-F00W00	6120	5995	56.9%	—	—
P2-F20W00	5994	5386	53.7%	2.1%	10.2%
P2-F40W00	5803	4925	48.8%	5.2%	17.8%
P2-F60W00	5541	4658	42.0%	9.5%	22.3%
P2-F80W00	5287	4387	35.5%	13.6%	26.8%
P2-F100W00	5060	4133	29.7%	17.3%	31.1%
P2-F100W20	4865	3849	24.7%	20.5%	35.8%
P2-F100W40	4632	3630	18.7%	24.3%	39.4%
P2-F100W60	4407	3426	13.0%	28.0%	42.9%
P2-F100W80	4164	3224	6.7%	32.0%	46.2%
P2-F100W100	4007	3060	2.7%	34.5%	49.0%
P2	3901	3353	—	—	—

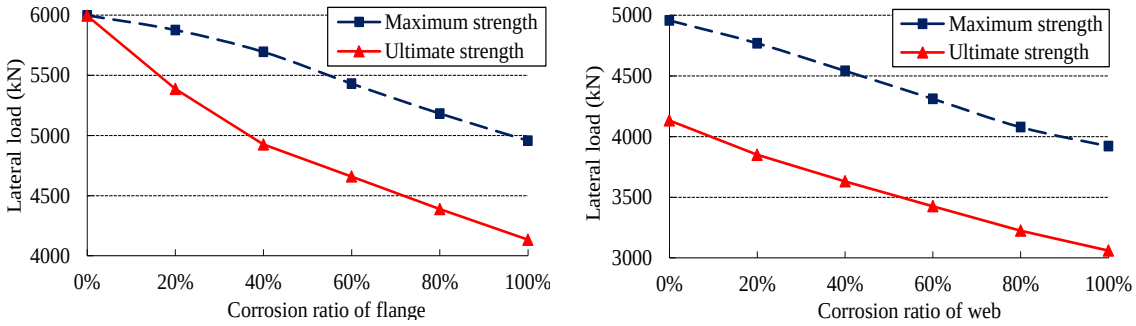

(a) Flange (b) Web

Fig. 12 Effect of corrosion ratio on load-carrying capacity

which indicates that corrosion ratio affects the ultimate strength more seriously. Compared with uncorroded specimen P2-F00W00, degradation ratio of the maximum strength for specimens P2-F100W00 and P2-F100W100 reaches 17.3% and 34.5%, respectively.

3.3 Uneven corrosion analysis of in-service pier

Corrosion pattern of steel plates consists of even corrosion mode and uneven corrosion mode. Even corrosion mode assumes that the steel plate corrodes uniformly, and the effect of corrosion is considered by changing the thickness of steel plates. Uneven corrosion mode represents that the corrosion of steel plates is local, asymmetric, which is often observed in actual bridge piers. Therefore, it is necessary to investigate the effect of uneven corrosion mode on the load-carrying capacity degradation of the piers.

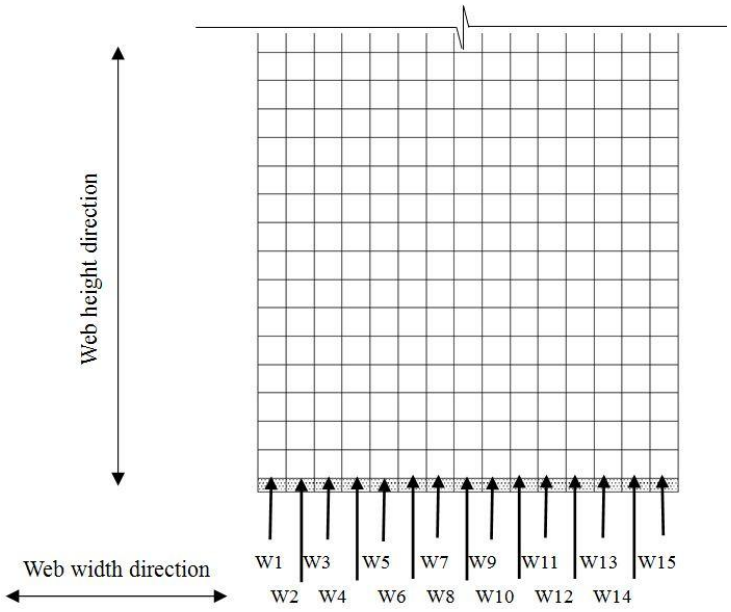

Fig. 13 Definition of corrosion position on web

As has been described in Section 2.2, beam-column element is employed to model flange, which cannot consider the effect of uneven corrosion mode. In contrast, plane stress element used for the modelling of web can account for the uneven corrosion of web. In the present analysis, it is assumed that the uneven corrosion begins from the tensile web, and propagates towards the compressive side. As illustrated in Fig. 13, 15 meshes are named sequentially as W1, W2, …, W15, firstly. Then five groups, that is, W1-W3, W1-W6, W1-W9, W1-W12, W1-W15 are defined as the corrosion group, which correspond to 20%, 40%, 60%, 80%, 100% of corrosion ratio, respectively. It should be noted that complete corrosion along plate thickness is assumed for each corrosion group.

Comparison of lateral load - lateral displacement curves of the specimens corresponding to different corrosion ratio of web is given in Fig. 14. With the increase in corrosion ratio of web, the maximum strength decreases in sequence. However, the two curves of specimens F100W100-W1-W12 (corrosion ratio = 80%) and F100W100-W1-W15 (corrosion ratio = 100%) almost overlap, which indicates that the variation of corrosion ratio doesn't affect the load-carry capacity so much in the case of severe corrosion. Fig. 15 shows the comparison of maximum strength versus web's corrosion ratio curves under different corrosion modes. It is observed that there exists a parabolic relationship between maximum strength and web's corrosion ratio in the case of uneven corrosion mode. For the same corrosion ratio, uneven corrosion mode results in more serious degradation of maximum strength than even corrosion mode. The possible reason can be explained as follows. In the case of even corrosion mode, the web near the pier base corrodes uniformly along the web width, and the corrosion ratio is dominated by the corrosion depth along web thickness. Because

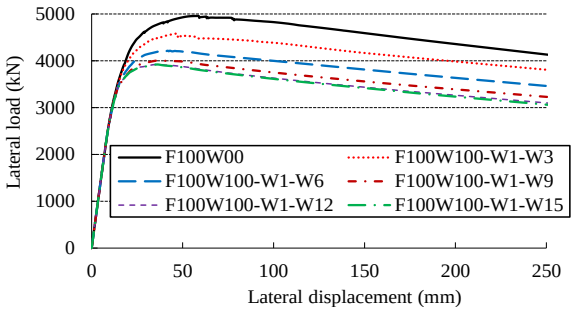

Fig. 14 Comparison of lateral load - lateral displacement curves of the specimens corresponding to different corrosion range of web

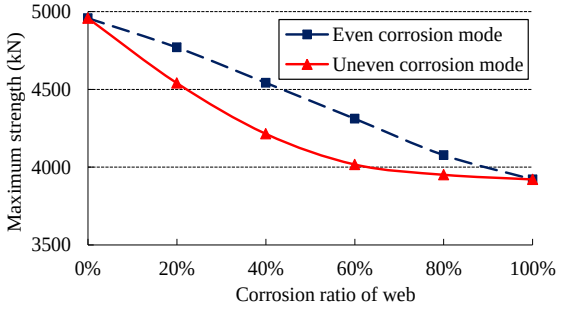

Fig. 15 Effect of corrosion ratio of web on load-carrying capacity under different corrosion modes

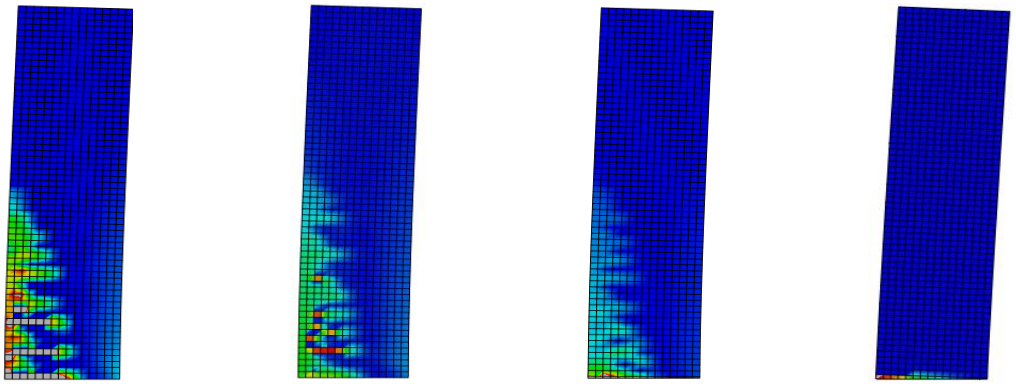

(a) P2 (b) P2-F00W00 (c) P2-F100W00 (d) P2-F100W100

Fig. 16 Comparison of principal tensile strain contour of concrete

the bending capacity provided by the web varies linearly along plate thickness, the maximum strength deteriorates linearly under even corrosion mode. In the case of uneven corrosion mode, corrosion ratio is controlled by the corrosion range along web width. It is well known that the bending capacity of web significantly differs along web width. For the same size of corroded web, the bending capacity provided by the tensile plate far away from the neutral axis is much larger than that of the steel plate located near the neutral axis. When the corrosion ratio exceeds 60%, the degradation of maximum strength becomes very gentle in the case of uneven corrosion mode.

3.4 Failure modes under different corrosion state

Fig. 16 shows the comparison of principal tensile strain contour of concrete for specimens P2, P2- F00W00, P2-F100W00 and P2-F100W100, which correspond to different corrosion state. It is observed that principal tensile strain of specimens P2, P2-F00W00 and P2-F100W00 is distributed within a wide range along column height, which displays a traditional concrete cracking pattern due to bending deformation. Compared with P2 and P2-F00W00, the cracking range of P2-F100W00 becomes a little narrower due to complete corrosion on flange. With respect to P2-F100W100, the principal tensile strain is extremely concentrated on the column base, where is a weakest region due to complete corrosion on both flange and web.

Fig. 17 shows the comparison of yield range of wrapped steel plates for specimens P2-F00W00, P2-F100W00 and P2-F100W100. A large range of steel plates in specimen P2-F00W00 yields due to the solid connection between steel plates and the foundation, which guarantees the bending moment at the column base to be efficiently transferred into the foundation. In contrast, the ability of specimens P2-F100W00 and P2-F100W100 to transfer the bending moments to the foundation are significantly affected by the corrosion of steel plates. That is why the yield range of the latter two specimens becomes smaller than that of the former specimen. When the steel plates near the pier base completely corrode, they can only provide constraint to the outward deformation of in-filled concrete. It is not possible for them to resist the lateral load any more. Consequently, the corrosion of steel plates near the pier base dominantly affects the load-carrying capacity of the piers.

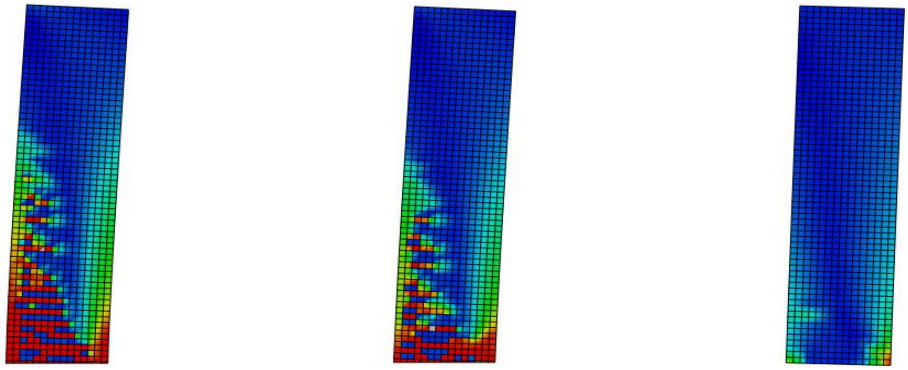

(a) P2-F00W00 (b) P2-F100W00 (c) P2-F100W100

Fig. 17 Comparison of von Mises stress contour of steel plates

4. Conclusions

This paper addressed the load-carrying capacity degradation of reinforced concrete piers due to corrosion of wrapped steel plates near the pier base. A series of parametric studies were carried out to investigate the effect of corrosion ratio and corrosion mode of steel plates on load-carrying capacity of the piers. Finally, the failure modes at different corrosion levels were discussed. The main conclusions are summarized as follows:

(1) The lateral load - lateral displacement curve obtained from numerical analysis coincides well with the test results, which indicates that the employed two-dimensional finite element formulation is accurate.
(2) With the increase in corrosion ratio of steel plates, the maximum strength of the specimens decreases rapidly. Both the maximum strength and ultimate strength decrease linearly as the increase of corrosion ratio under even corrosion mode.
(3) To what extent the maximum strength of the specimens can be improved mainly depends on the corrosion state of the steel plates. When the steel plates near the pier base completely corrode, the maximum strength is only increased by 2.7%.
(4) There exists a parabolic relationship between maximum strength and web's corrosion ratio in the case of uneven corrosion mode. For the same corrosion ratio, uneven corrosion mode results in more serious degradation of maximum strength than even corrosion mode.
(5) The principal tensile strain of concrete and yield range of steel plates are distributed within a wide range in the case of slight corrosion, and they are concentrated on the pier base when complete corrosion occurs.
(6) With the increase in corrosion ratio, the ability to transfer the bending moments to the foundation is greatly reduced. The corrosion of steel plates near the pier base has a dominant effect on the load-carrying capacity of the piers.

The present research results in this paper indicate that the uneven corrosion mode has a more serious effect on the load-carrying capacity of the piers. Furthermore, the deterioration of interface behavior between steel plates and concrete cannot be accounted for in 2-D finite element analysis modelling. Therefore, it is necessary to carry out local corrosion analysis by employing 3-D finite element formulation which will be reported in near future.

References

ABAQUS analysis user's manual (2010), SIMULIA, Providence, RI, USA.

Fan, J.S., Li, Q.W., Nie, J.G. and Zhou, H. (2014), "Experimental study on the seismic performance of 3d joints between concrete-filled square steel tubular columns and composite beams", *J. Struct. Eng., ASCE*, **140**(12), 04014094(13).

Fang, C.Q. and Kou, X.J. (2005), "The effect of steel corrosion on bond strength in concrete structures", *J. Shanghai Jiaotong Univ.* (*Sci.*), **E-10**(4), 436-440.

Gao, S.B. and Ge, H.B. (2007), "Numerical simulation of hollow and concrete-filled steel columns", *Adv. Steel Const., Int. J.*, **3**(3), 668-678.

GB50011-2010 (2010), Code for seismic design of buildings, China Architecture and Building Press, Beijing, China. [In Chinese]

Han, L.H., Tan, Q.H. and Song, T.Y. (2015), "Fire performance of steel reinforced concrete columns", *J. Struct. Eng., ASCE*, **141**(4), 04014128(13).

Hou, C., Han, L.H. and Zhao, X.L. (2013), "Full-range analysis on square CFST stub columns and beams under loading and chloride corrosion", *Thin-Wall. Struct.*, **68**, 50-64.

Kaita, T., Appuhamy, J.M.R.S., Ohga, M. and Fujii, K. (2012), "An enhanced method of predicting effective thickness of corroded steel plates", *Steel Compos. Struct., Int. J.*, **12**(5), 379-393.

Kang, W.H., Uy, B., Tao, Z. and Hicks, S. (2015), "Design strength of concrete-filled steel columns", *Adv. Steel Constr.*, **11**(2), 165-184.

Karagah, H., Shi, C. and Dawood, M. (2015), "Experimental investigation of short steel columns with localized corrosion", *Thin-Wall. Struct.*, **87**, 191-199.

Khedmati, R.M., Esmaeil Nouri, Z.H.M. and Roshanali, M.M. (2011), "An effective proposal for strength evaluation of steel plates randomly corroded on both sides under uniaxial compression", *Steel Compos. Struct., Int. J.*, **11**(3), 183-205.

Maekawa, K., Takemura, J., Irawan, P. and Irie, M. (1993), "Continuum fracture in concrete nonlinearity under triaxial confinement", *Proc. Japan Society Civ. Eng.* (*JSCE*), **18**(46), 113-122.

Saito, S., Kameyama, Y., Hikosaka, H. and Isibashi, O. (1996), "Finite element analysis of reinforced concrete bridge piers retrofitted with steel jacketing", *Tech. Rep. Kyushu Univ.*, **69**(3), 231-237. [In Japanese]

Sharifi, Y. and Paik, J.K. (2011), "Ultimate strength reliability analysis of corroded steel-box girder bridges", *Thin-Wall. Struct.*, **49**(1), 157-166.

Shi, C., Karagah, H., Dawood, M. and Belarbi, A. (2014), "Numerical investigation of H-shaped short steel piles with localized severe corrosion", *Eng. Struct.*, **73**, 114-124.

Silva, J. and Garbatov, Y. (2013), "Ultimate strength assessment of rectangular steel plates subjected to a random localized corrosion degradation", *Eng. Struct.*, **52**, 295-305.

Wan, M.L. and Han, J.Y. (1995), *Technology of Strengthening Concrete Structure*, Architecture and Building Press, Beijing, China. [In Chinese]

Wang, X.H. and Liu, X.L. (2012), "Effects of length and location of steel corrosion on the behavior and load capacity of reinforced concrete columns", *J. Shanghai Jiaotong Univ.* (*Sci.*), **17**(4), 391-400.

Zhang, B. (2011), *Effect of Corrosion on the Performance of Concrete-filled Steel Tubes*, Chongqing Jiaotong University, Chongqing, China. [In Chinese]

CC